Enhancing Photovoltaic Performance of Nonfused-Ring Electron Acceptors via Asymmetric End-group Engineering and Noncova-lently Conformational Locks

Bo Liu[1], Congqi Li[2], Xiaobin Gu[2], Yinghui Han[2], Zhixiang Wei[3], Yunhao Cai[2], Xin Zhang[2], and Yanping Huo[1]

[1]Guangdong University of Technology
[2]University of the Chinese Academy of Sciences
[3]National Center for Nanoscience and Technology

October 3, 2023

Abstract

By employing the asymmetric end-group engineering, an asymmetric nonfused-ring electron acceptors (NFREAs) was designed and synthesized. Compared with the symmetric analogs (NoCA-17 and NoCA-18), NoCA-19 possesses broader light absorption range, more coplanar π-conjugated backbone, and appropriate crystallinity according to the experimental and theoretical results. The organic solar cells based on J52:NoCA-19 exhibited a power conversion efficiency as high as 12.26%, which is much higher than those of J52:NoCA-17 (9.50%) and J52:NoCA-18 (11.77%), mainly due to more efficient exciton dissociation, better and balanced charge mobility, suppressed recombination loss, shorter charge extraction time, longer charge carrier lifetimes, and more favorable blend film morphology. These findings demonstrate the great potential of asymmetric end-group engineering in exploring low-cost and high-performance NFREAs.

Cite this paper:*Chin. J. Chem.* **2023** , *41* , XXX—XXX. **DOI: 10.1002/cjoc.202300XXX**

Enhancing Photovoltaic Performance of Nonfused-Ring Electron Acceptors via Asymmetric End-group Engineering and Noncovalently Conformational Locks[+]

Bo Liu,[a ,b] Congqi Li,[b] Xiaobin Gu,[b]Yinghui Han,*[,c] Zhixiang Wei,[d] Yunhao Cai,[b] Xin Zhang*[,b] and Yanping Huo*[,a]

[a] School of Chemical Engineering and Light Industry, Guangdong University of Technology, Guangzhou 510006, China[b] College of Materials Science and Opto-Electronic Technology & Center of Materials Science and Optoelectronics Engineering & CAS Center for Excellence in Topological Quantum Computation & CAS Key Laboratory of Vacuum Physics, University of Chinese Academy of Sciences, Beijing 100049, China[c] College Resources and Environment, University of Chinese Academy of Sciences, Beijing 100049, China[d] Center for Excellence in Nanoscience (CAS) & Key Laboratory of Nanosystem and Hierarchical Fabrication (CAS), National Center for Nanoscience and Technology, Beijing 100190, China

Keywords

Organic solar cells | Nonfused-ring electron acceptors | Asymmetric end-group engineering | Noncovalently conformational lo

Comprehensive Summary

By employing the asymmetric end-group engineering, an asymmetric nonfused-ring electron acceptors (NFREAs) was desig

Background and Originality Content

Organic solar cells (OSCs) have gained attention for their light weight, adjustable absorption range, flexibility, and solution processability.[1-3]Recent advancements in this field have been primarily driven by polymeric and small-molecule donors/acceptors, with the power conversion efficiencies (PCEs) surpassing 19% for single-junction devices.[4-14] Among the high-performance acceptor materials, the acceptor-donor-acceptor (A-D-A) and A-DA'D-A-structured fused-ring electron acceptors (FREAs), exemplified by Y6 and ITIC respectively, stand out.[15-20] With the aim of exploring superior acceptors, considerable research has focused on molecular engineering, such as π-conjugated extension, side-chain engineering, end-group halogenation, and isomerization, to regulate the light harvesting abilities, energy levels, and packing behaviors of FREAs.[21-24] In addition, asymmetric strategy serves as a key molecular design approach in enhancing the dipole moment and dielectric constant while reducing the exciton binding energy, thereby promoting exciton dissociation and charge transport.[25, 26]

With the rapid development of FREAs, another type of nonfused-ring electron acceptors (NFREAs), aimed at reducing product costs, has emerged.[27-32] This type of acceptors typically possess a partially or completely non-fused ring cores, greatly simplifying molecular design and opening the opportunity for constructing cost-effective acceptor materials.[33, 34] However, the additionally introduced rotatable σ -single bonds can result in conformational isomers and twisted backbones. To address this issue, large steric hindrance of side-chains and weak intramolecular interactions (also known as noncovalently conformational locks, NoCLs) are introduced in molecular design to lock-in the conformation, thereby eliminating conformational isomers and achieving a highly coplanar π -conjugated backbones.[35-42] Recently, we reported a PhO4T-series of symmetric NFREAs, demonstrating higher figure-of-merit values than those of FREAs, due to their simple structures and concise synthesis routes.[43] However, the PCEs of NFREAs have still lagged far behind those of FREAs. Therefore, how to rationally design NFREAs for low-cost and high-performance OSCs remains challenging.

Herein, asymmetric engineering was employed to construct a new NFREA, namely NoCA-19, with two distinct end-groups (2-(5,6-dichloro-3-oxo-2,3-dihydro-1H -inden-1-ylidene)malononitrile, IC-2Cl; and 2-(6,7-difluoro-3-oxo-2,3-dihydro-1H -cyclopenta[b]naphthalen-1-ylidene)malononitrile, NC-2F) on the basis of two symmetric NFREAs (one is previously reported acceptor NoCA-17, and another one is newly synthesized acceptor NoCA-18) (Figure 1a). Experimental and theoretical results show that asymmetric acceptor NoCA-19 possesses broader light absorption range, more coplanarπ-conjugated backbone, and appropriate crystallinity, compared to the two symmetric acceptors. When blending with the polymer donor J52, the NoCA-19-based blend film afforded more balanced charge mobility, suppressed recombination loss, shorter charge extraction time, and more favorable morphology. Therefore, the asymmetric NFREA NoCA-19-based OSCs achieved the highest PCE of 12.26% among the three blend systems. This work highlights the importance of asymmetric end-group engineering in exploring low-cost and high-performance NFREAs.

Results and Discussion

Synthesis and characterization

As depicted in Scheme S1, the three NFREAs were synthesized in one-pot Knoevenagel condensation reaction, and then separated individually by column chromatography. The synthesis route is shown in Scheme S1, and the detailed synthesis procedures and the ^{1}H-/^{13}C-NMR spectra were given in Supporting Information. All the three acceptors show good solubility in common solvents, such as chloroform, toluene, and chlorobenzene.

The UV–vis absorption of these three acceptors in both dilute chloroform solution and thin-film state are shown in Figures 1b and 1c, and the corresponding optical parameters are summarized in Table 1. In dilute chloroform solutions, the shapes of the normalized absorption curves for three NFREAs are almost identical

in the range of 550–850 nm (Figure 1b). The maximum absorption peaks at 724 nm for NoCA-17 and 734 nm for NoCA-18 indicate a stronger electron-withdrawing ability of NC-2F

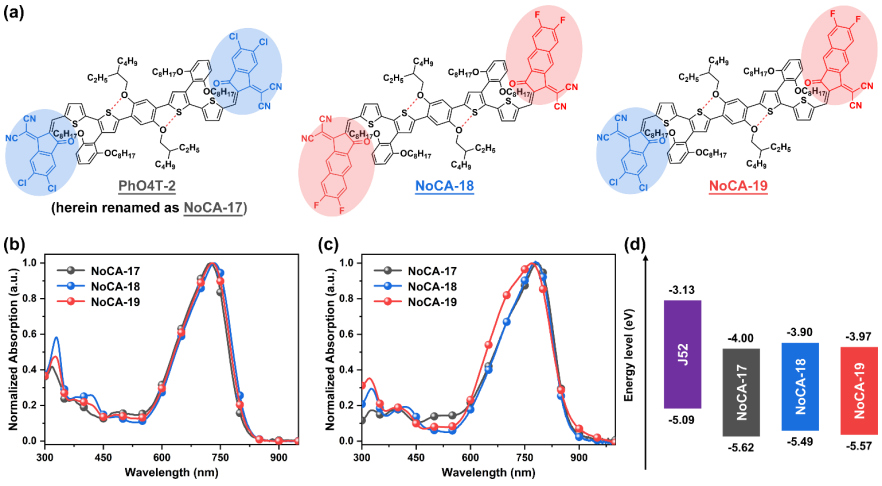

Figure 1 (a) Chemical structures, normalized dilute solution (b) and thin film (c) optical absorption spectra of the three NRFEAs. (d) Energy level diagram of donor and acceptor materials in this work.

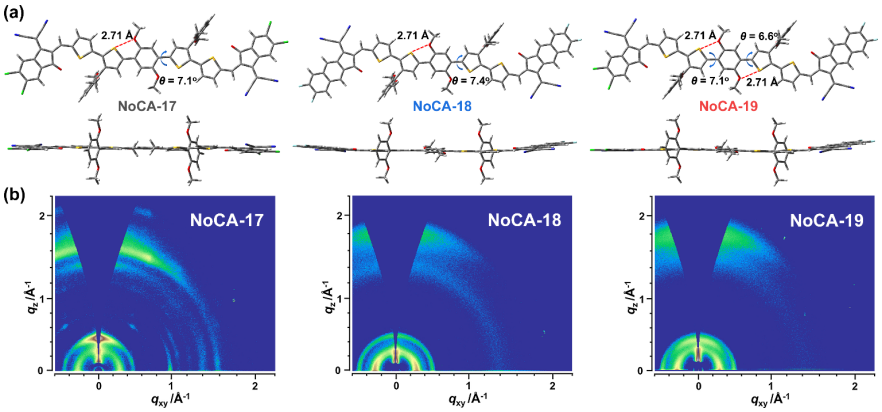

Figure 2 (a) Optimized geometries (top: top view; bottom: side view) of the three NFREAs. (b) 2D-GIWAXS patterns of neat NoCA-17, NoCA-18, and NoCA-19 films.

compared to IC-2Cl, leading to a more efficient intramolecular charge transfer effect. Accordingly, NoCA-19 displays a blue-shifted absorption peak (728 nm) in comparison NoCA-18. Both symmetric acceptors, NoCA-17 and NoCA-18, in the thin film exhibit comparable absorption spectra. In contrast, the asymmetric acceptor NoCA-19 demonstrates a broadening of the absorption spectrum in the high-energy region, indicating a unique stacking arrangement in the solid state.

Table 1 Basic properties of NoCA-17, NoCA-18, and NoCA-19

NFREAs	$\lambda_{abs.max}{}^{sol.}$ [nm]	$\lambda_{abs.max}{}^{film}$ [nm]	$E_{HOMO}/E_{LUMO}{}^{a}$ [eV]	$E_{HOMO}/E_{LUMO}{}^{b}$ [eV]
NoCA-17	724	784	-5.62/-4.00	-5.25/-3.30
NoCA-18	734	781	-5.49/-3.90	-5.17/-3.22

NFREAs	$\lambda_{abs.max}^{sol.}$ [nm]	$\lambda_{abs.max}^{film}$ [nm]	E_{HOMO}/E_{LUMO} [a] [eV]	E_{HOMO}/E_{LUMO} [b] [eV]
NoCA-19	728	770	-5.57/-3.97	-5.21/-3.27

[a] Calculated by CV measurements.[b] Derived from DFT calculations.

Furthermore, cyclic voltammetry (CV) was employed to estimate the energy levels of the NFREAs in solid state. The highest occupied molecular orbital (HOMO) and the lowest unoccupied molecular orbital (LUMO) energy levels derived from the oxidation/reduction onsets of the CV curves (Figure S1) are -5.62/-4.00, -5.49/-3.90, and -5.57/-3.97 eV for NoCA-17, NoCA-18, and NoCA-19, respectively (Figure 1d and Table 1). Moreover, the trend of DFT calculated $E_{HOMO/LUMO}$ values for three NFREAs is well consistent with CV results (Figure S2).

The optimized molecular geometries of the three NFREAs were investigated by performing density function theory (DFT) calculations at the B3LYP/6-31G(d,p) level. The intramolecular distances between the sulfur atom of the thiophene ring and oxygen atom of the phenylalkoxy motif are found to be ˜2.71 Å for all these three acceptors (Figure 2a), much shorter than the sum of the van der Waals radius ($r_{w, S\cdots O}$ = 3.25 Å), indicating the existence of S···O NoCLs. The dihedral angles between the central phenyl core and the adjacent thiophene ring are 7.1° and 7.4° for NoCA-17 and NoCA-18, respectively. In the case of NoCA-19, the dihedral angles decrease slightly to 7.1/6.6°, indicating a more coplanar π -conjugated backbone due to asymmetric substitution of end-groups.

The packing behaviors in neat films were explored by measuring the two-dimensional grazing incidence wide-angle X-ray scattering (2D-GIWAXS). In the in-plane (IP) direction, the neat NoCA-17 film exhibits a lamellar packing diffraction peak at q_{xy} = 0.30 Å^{-1} (d˜ 22.67 A), as shown in Figures 1b and S3. Additionally, the π -π stacking diffraction signal is observed in the out-of-plane (OOP) direction at q_z = 1.61 Å^{-1} (d ˜ 3.90 Å), suggesting the predominant face-on orientation of NoCA-17. In the neat NoCA-18 film, the lamellar packing diffraction peak is also observed at q_{xy} = 0.30 Å^{-1} in the IP direction, while the π -π diffraction peak is located at q_z = 1.78 Å^{-1} (d˜ 3.53 Å), indicating that the end-group NC-2F can enhance intermolecular interactions and achieve tighter packing. Surprisingly, the neat NoCA-19 film exhibits a balanced π -π stacking distance (q_z = 1.74 Å^{-1}, d ˜ 3.62 Å), which is closer than NoCA-17 and looser than NoCA-18. The results demonstrate that the asymmetric end-group engineering can effectively regulate the packing behaviors in the neat films, enabling NoCA-19 to possess moderate π -π stacking distance and appropriate crystallinity.

Photovoltaic properties

To investigate the photovoltaic performance of the three NFREAs, OSC devices were fabricated with a conventional structure of ITO/PEDOT:PSS/active layer/PDINO/Al based on J52:NoCA-series acceptors blends. The current density-voltage ($J-V$) characteristics are shown in Figure 3a. The detailed device parameters and the optimization process can be found in Tables 2 and S1-S3. The optimized device based on J52:NoCA-17 exhibits an inferior PCE of 9.50%, with an open circuit voltage (V_{oc}) of 0.804 V, a short circuit current density (J_{sc}) of 21.55 mA cm^{-2}, and a fill factor (FF) of 54.81%. Furthermore, the device based on J52:NoCA-18 shows a decrease in V_{oc} (0.792 V) but an improvement in J_{sc} (22.72 mA cm^{-2}) and FF (65.51%), resulting in a higher PCE of 11.77%. Impressively, the NoCA-19 based device exhibits the champion PCE of 12.26% with an much higher J_s (23.11 mA cm^{-2}) and FF (67.11%). External quantum efficiency (EQE) measurements were carried out to verify the above J_{sc} values (Figure 3b). The integrated J_{sc} values of the devices based on J52:NoCA-17, J52:NoCA-18, and J52:NoCA-19 are 20.80 mA cm^{-2}, 21.90 mA cm^{-2}, and 22.16 mA cm^{-2}, respectively, The corresponding mismatches are less than 5%, as compared to the values from $J-V$ characteristics.

Space charge limited current method was used to evaluate charge transport properties in the three blend films, as shown in Figure S4. The hole mobility (μ_h) and electron mobility (μ_e) were calculated to be 8.74 × 10^{-4} and 6.69 x 10^{-4}cm^2 V^{-1} s^{-1} for the NoCA-19 blend film, respectively. These values were found to

be much higher than those of the NoCA-17-based blend film (6.42 x 10^{-4} and 4.10 x 10^{-4} cm^2 V^{-1} s^{-1}) and NoCA-18-based blend film (7.81 x 10^{-4} and 5.85 x 10^{-4} cm^2 $V^{-1}s^{-1}$). Furthermore, the J52:NoCA-19 blend film exhibited more balanced charge carrier mobilities (μ_h/μ_e = 1.31) compared to the other two blends, which may contribute to the observed improvement in FF.

Table 2 Photovoltaic parameters of OSCs based on PM6:NFREAs under AM1.5G illumination, 100 mW cm^{-2}.

Active layers	V_{oc} [a] [V]	J_{sc} [mA cm^{-2}]	FF [%]	PCE [%]
J52:NoCA-17	0.804 (0.803±0.001)	21.55 (21.48±0.17)	54.81 (54.52±0.44)	9.50 (9.40±0.07)
J52:NoCA-18	0.792 (0.792±0.001)	22.72 (22.60±0.15)	65.51 (65.22±0.57)	11.77 (11.67±0.10)
J52:NoCA-19	0.841 (0.790±0.001)	23.11 (23.07±0.10)	67.11 (67.08±0.26)	12.26 (12.22±0.02)

[a] The average values shown in parentheses were obtained from 15 devices.

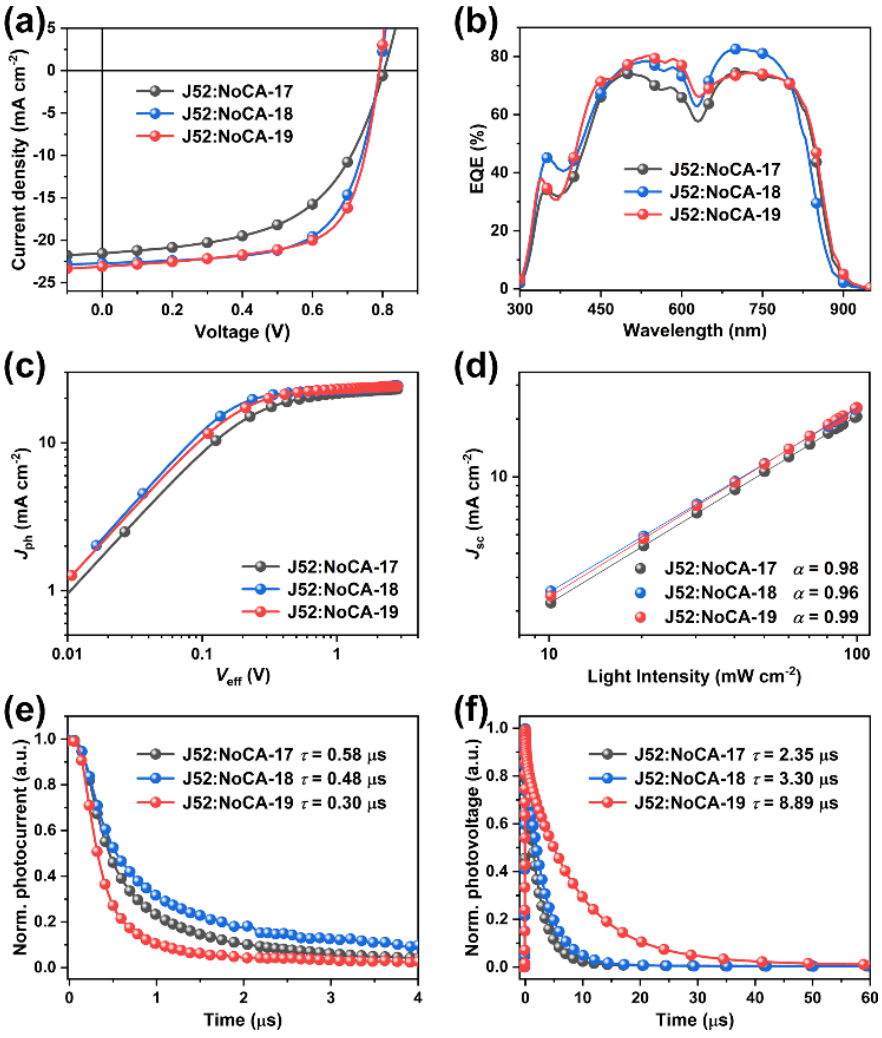

Figure 3 (a) J - V characteristics, (b) EQE responses, (c) J_{ph}-V_{eff}, (d) J_{sc}-P_{light}, (e) TPC, and (f) TPV measurements of the optimized OSCs based on J52:NoCA-17, J52:NoCA-18, and J52:NoCA-19.

To deep understand the variation in photovoltaic performance among the three OSC devices, charge generation and recombination were systematically studied. The photocurrent density (J_{ph}) versus effective voltage (V_{eff}) curves were measured to investigate the exciton dissociation and charge extraction mechanism. The exciton dissociation probability $P(E, T)$ can be reflected by the ratio of J_{ph} to J_{sat}, where J_{sat} is defined as the saturation J_{ph} at a sufficiently high V_{eff}, indicating that all photogenerated excitons can be dissociated into free carriers and almost totally collected by the individual electrodes. As shown in Figure 3c, the P_{diss} values were calculated as 95.1%, 96.0%, and 97.3% for the NoCA-17, NoCA-18, and NoCA-19-based devices, respectively. The higher P (E, T) suggests that the J52:NoCA-19 blend film exhibits more efficient exciton dissociation and charge collection, which is consistent with the higher J_{sc} value. In addition, the J - V curves were measured under various light intensities (P_{light}) to investigate the charge recombination properties. The relationship between J_{sc} and P_{light} relationship can be described by J_{sc} [?] $P_{light}{}^{\alpha}$, where the bimolecular recombination can be completely suppressed when the ? value approaches unity. As shown in Figure 3d, the α values were calculated as 0.98, 0.96, and 0.99 for the NoCA-17, NoCA-18, and NoCA-19-based devices, respectively. The higher α for the NoCA-19 blend system indicates suppressed bimolecular recombination, which may contribute to the higher J_{sc} and FF relative to the other two devices.

The charge extraction and recombination processes were further investigated by measuring the transient photocurrent (TPC) and transient photovoltage (TPV) decay kinetics of three devices. The charge sweep-out times at short-circuit condition were evaluated to be 0.58, 0.48, and 0.30 μs for NoCA-17, NoCA-18, and NoCA-19 based blends, respectively, indicating higher charge extraction efficiency and higher electron mobility (Figure 3e). The carrier lifetimes obtained from the decay traces of TPV measurements (Figure 3f) were 2.35, 3.30, and 8.89 μs for NoCA-17, NoCA-18, and NoCA-19 based devices, respectively. At open-circuit condition, the relatively longer lifetime of free carriers may imply less recombination. These above results are consistent to the improved J_{sc} and FF in J52:NoCA-19 based device.

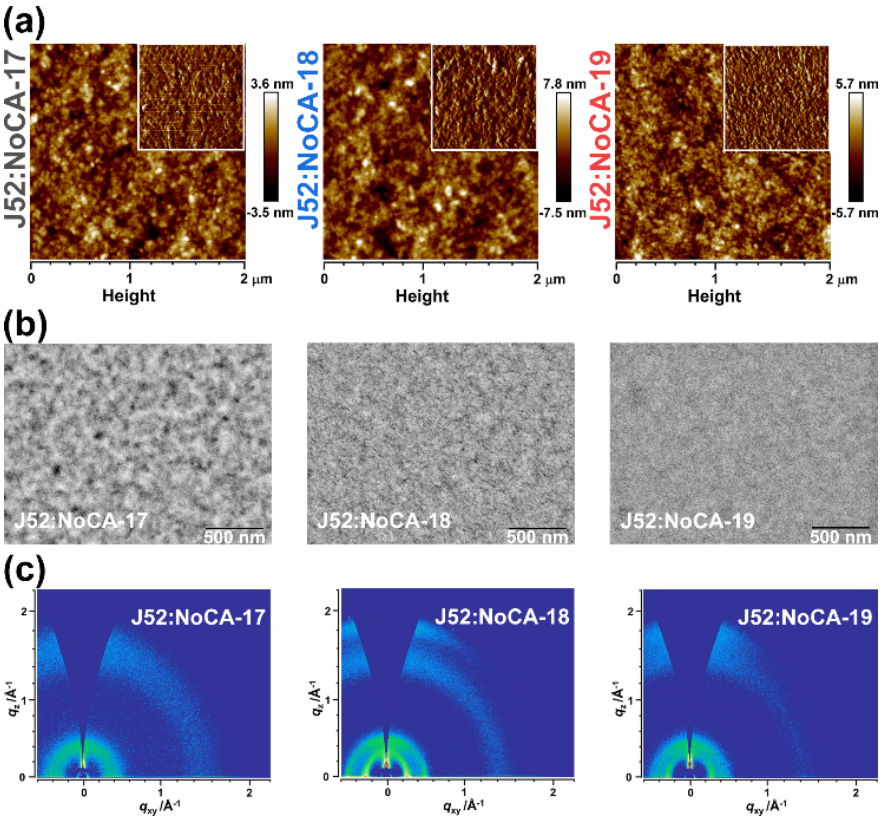

Figure 4 (a) Tapping-mode AFM height images (2 μm × 2 μm) (insets are phase images of 1 μm × 1 μm size), (b) TEM images, and (c) 2D-GIWAXS patterns of J52:NoCA-17, J52:NoCA-18, and J52:NoCA-19 blend films.

Morphology investigation

The surface and bulk morphologies of blend films were investigated by atomic force microscopy (AFM) and transmission electron microscopy (TEM). As shown in Figure 4a, the J52:NoCA-19 blend film exhibits a uniform surface with a higher root-mean-square (R_q) surface roughness of 1.57 nm compared to the J52:NoCA-17 (1.09 nm) and J52:NoCA-18 (1.43 nm) blend films. Furthermore, Figure 4b shows that the J52:NoCA-19 blend film exhibits smaller domain sizes and nano-scale phase separation. To provide further insight into the molecular packing in the blend films, 2D-GIWAXS was employed (Figures 4c and S5). The NoCA-17-based blend film demonstrates overlapping lamellar packing diffraction peaks with the polymer J52. Interestingly, the lamellar packing diffraction peaks of the acceptors in the NoCA-18 and NoCA-19-based blend films remain clear, indicating that the order packings of NoCA-18 and NoCA-19 were not vulnerable to be disturbed when blending with J52. This features in film morphology are beneficial for charge transport and thus device performance.

Conclusions

In conclusion, the asymmetric end-group engineering was employed to construct a new NFREA, namely NoCA-19 containing two distinct end-groups, IC-2Cl and NC-2F. Together with two symmetrical NFREAs (NoCA-17 and NoCA-18), experimental and theoretical studies were systematically carried out, showing that asymmetric acceptor NoCA-19 possesses broad light absorption range, more coplanar π-conjugated backbone, and appropriate crystallinity. The NoCA-19-based device delivered a champion PCE of 12.26%, mainly due to the best and most balanced carrier mobility, least charge recombination, shortest charge extraction time, and most favorable morphology among the three blend systems. This work sheds light on the potential of asymmetric end-group engineering in designing low-cost and high-performance NFREAs.

Supporting Information

The supporting information for this article is available on the WWW under https://doi.org/10.1002/cjoc.2023xxxxx.

Acknowledgement

B. Liu and C. Li contributed equally to this work. The authors acknowledge the financial support from the NSFC (2197505, U2001222, 52103352, 52120105006, and 51925306), National Key R&D Program of China (2018FYA 0305800), Key Research Program of Chinese Academy of Sciences (XDPB08-2), the Youth Innovation Promotion Association of Chinese Academy of Sciences (2022165), and the Fundamental Research Funds for the Central Universities. DFT results described in this article were obtained from the National Supercomputing Centre in Shenzhen (Shenzhen Cloud Computing Centre).

References

[1] Lu, L.; Zheng, T.; Wu, Q.; Schneider, A. M.; Zhao, D., Yu, L. Recent Advances in Bulk Heterojunction Polymer Solar Cells. *Chem. Rev.* **2015**, *115*, 12666–12731. [2] Inganäs, O. Organic Photovoltaics over Three Decades. *Adv. Mater.* **2018**, *30*, 1800388. [3] Karki, A.; Gillett, A. J.; Friend, R. H., Nguyen, T.-Q. The Path to 20% Power Conversion Efficiencies in Nonfullerene Acceptor Organic Solar Cells. *Adv. Energy Mater.* **2021**, *11*, 2003441. [4] Cai, Y.; Huo, L., Sun, Y. Recent Advances in Wide-Bandgap Photovoltaic Polymers. *Adv. Mater.* **2017**, *29*, 1605437. [5] Wan, X.; Li, C.; Zhang, M., Chen, Y. Acceptor–donor–acceptor type molecules for high performance organic photovoltaics – chemistry and mechanism. *Chem. Soc. Rev.* **2020**, *49*, 2828-2842. [6] Jin, K.; Xiao, Z., Ding, L. D18, an eximious solar polymer! *J. Semicond.* **2021**, *42*, 010502. [7] Gao, W.; Qi, F.; Peng, Z.; Lin, F. R.; Jiang, K.; Zhong, C.; Kaminsky, W.; Guan, Z.; Lee, C.-S.; Marks, T. J.; Ade, H., Jen, A. K. Y. Achieving 19% Power Conversion Efficiency in Planar-Mixed Heterojunction Organic Solar Cells Using a Pseudosymmetric Electron Acceptor. *Adv. Mater.* **2022**, *34*, 2202089. [8] Liu, Y.;

Liu, B.; Ma, C.-Q.; Huang, F.; Feng, G.; Chen, H.; Hou, J.; Yan, L.; Wei, Q.; Luo, Q.; Bao, Q.; Ma, W.; Liu, W.; Li, W.; Wan, X.; Hu, X.; Han, Y.; Li, Y.; Zhou, Y.; Zou, Y.; Chen, Y.; Li, Y.; Chen, Y.; Tang, Z.; Hu, Z.; Zhang, Z.-G., Bo, Z. Recent progress in organic solar cells (Part I material science). *Sci. China Chem.***2022**, *65*, 224-268. [9] Zheng, Z.; Wang, J.; Bi, P.; Ren, J.; Wang, Y.; Yang, Y.; Liu, X.; Zhang, S., Hou, J. Tandem Organic Solar Cell with 20.2% Efficiency.*Joule* **2022**, *6*, 171-184. [10] Zhu, L.; Zhang, M.; Xu, J.; Li, C.; Yan, J.; Zhou, G.; Zhong, W.; Hao, T.; Song, J.; Xue, X.; Zhou, Z.; Zeng, R.; Zhu, H.; Chen, C.-C.; MacKenzie, R. C. I.; Zou, Y.; Nelson, J.; Zhang, Y.; Sun, Y., Liu, F. Single-junction organic solar cells with over 19% efficiency enabled by a refined double-fibril network morphology. *Nat. Mater.* **2022**, *21*, 656-663. [11] Sun, R.; Wu, Y.; Yang, X.; Gao, Y.; Chen, Z.; Li, K.; Qiao, J.; Wang, T.; Guo, J.; Liu, C.; Hao, X.; Zhu, H., Min, J. Single-Junction Organic Solar Cells with 19.17% Efficiency Enabled by Introducing One Asymmetric Guest Acceptor. *Adv. Mater.* **2022**, *34*, 2110147. [12] Gao, J.; Yu, N.; Chen, Z.; Wei, Y.; Li, C.; Liu, T.; Gu, X.; Zhang, J.; Wei, Z.; Tang, Z.; Hao, X.; Zhang, F.; Zhang, X., Huang, H. Over 19.2% Efficiency of Organic Solar Cells Enabled by Precisely Tuning the Charge Transfer State Via Donor Alloy Strategy. *Adv. Sci.* **2022**, *9*, 2203606. [13] Wei, Y.; Chen, Z.; Lu, G.; Yu, N.; Li, C.; Gao, J.; Gu, X.; Hao, X.; Lu, G.; Tang, Z.; Zhang, J.; Wei, Z.; Zhang, X., Huang, H. Binary Organic Solar Cells Breaking 19% via Manipulating the Vertical Component Distribution. *Adv. Mater.* **2022**, *34*, 2204718. [14] Li, C.; Gu, X.; Chen, Z.; Han, X.; Yu, N.; Wei, Y.; Gao, J.; Chen, H.; Zhang, M.; Wang, A.; Zhang, J.; Wei, Z.; Peng, Q.; Tang, Z.; Hao, X.; Zhang, X., Huang, H. Achieving Record-Efficiency Organic Solar Cells upon Tuning the Conformation of Solid Additives. *J. Am. Chem. Soc.* **2022**, *144*, 14731-14739. [15] Wang, J.; Xue, P.; Jiang, Y.; Huo, Y., Zhan, X. The principles, design and applications of fused-ring electron acceptors. *Nat. Rev. Chem.* **2022**, *6*, 614-634. [16] Wang, J., Zhan, X. From Perylene Diimide Polymers to Fused-Ring Electron Acceptors: A 15-Year Exploration Journey of Nonfullerene Acceptors. *Chin. J. Chem.* **2022**, *40*, 1592-1607. [17] Wei, Q.; Liu, W.; Leclerc, M.; Yuan, J.; Chen, H., Zou, Y. A-DA'D-A non-fullerene acceptors for high-performance organic solar cells. *Sci. China Chem.* **2020**, *63*, 1352-1366. [18] Lin, Y.; Wang, J.; Zhang, Z.-G.; Bai, H.; Li, Y.; Zhu, D., Zhan, X. An Electron Acceptor Challenging Fullerenes for Efficient Polymer Solar Cells. *Adv. Mater.* **2015**, *27*, 1170-1174. [19] Yuan, J.; Zhang, Y.; Zhou, L.; Zhang, G.; Yip, H.-L.; Lau, T.-K.; Lu, X.; Zhu, C.; Peng, H.; Johnson, P. A.; Leclerc, M.; Cao, Y.; Ulanski, J.; Li, Y., Zou, Y. Single-Junction Organic Solar Cell with over 15% Efficiency Using Fused-Ring Acceptor with Electron-Deficient Core. *Joule* **2019**, *3*, 1140–1151. [20] Gu, X.; Zhang, X., Huang, H. Oligomerized Fused-Ring Electron Acceptors for Efficient and Stable Organic Solar Cells. *Angew. Chem. Int. Ed.* **2023**, *62*, e202308496. [21] Xu, T.; Luo, Z.; Ma, R.; Chen, Z.; Dela Pena, T. A.; Liu, H.; Wei, Q.; Li, M.; Zhang, C. e.; Wu, J.; Lu, X.; Li, G., Yang, C. High-Performance Organic Solar Cells Containing Pyrido[2,3-b]quinoxaline-Core-Based Small-Molecule Acceptors with Optimized Orbit Overlap Lengths and Molecular Packing. *Angew. Chem. Int. Ed.* **2023**, *62*, e202304127. [22] Zhang, X.; Qin, L.; Liu, X.; Zhang, C.; Yu, J.; Xiao, Z.; Zheng, N.; Wang, B.; Wei, Y.; Xie, Z.; Wu, Y.; Wei, Z.; Wang, K.; Gao, F.; Ding, L., Huang, H. Enhancing the Photovoltaic Performance of Triplet Acceptors Enabled by Side-Chain Engineering. *Sol. RRL***2021**, *5*, 2100522. [23] Liang, H.; Bi, X.; Chen, H.; He, T.; Lin, Y.; Zhang, Y.; Ma, K.; Feng, W.; Ma, Z.; Long, G.; Li, C.; Kan, B.; Zhang, H.; Rakitin, O. A.; Wan, X.; Yao, Z., Chen, Y. A rare case of brominated small molecule acceptors for high-efficiency organic solar cells. *Nat. Commun.***2023**, *14*, 4707. [24] Wang, J.; Zhang, J.; Xiao, Y.; Xiao, T.; Zhu, R.; Yan, C.; Fu, Y.; Lu, G.; Lu, X.; Marder, S. R., Zhan, X. Effect of Isomerization on High-Performance Nonfullerene Electron Acceptors. *J. Am. Chem. Soc.* **2018**, *140*, 9140–9147. [25] Li, C.; Fu, H.; Xia, T., Sun, Y. Asymmetric Nonfullerene Small Molecule Acceptors for Organic Solar Cells. *Adv. Energy Mater.***2019**, *9*, 1900999. [26] Li, D.; Sun, C.; Yan, T.; Yuan, J., Zou, Y. Asymmetric Non-Fullerene Small-Molecule Acceptors toward High-Performance Organic Solar Cells. *ACS Cent. Sci.* **2021**, *7*, 1787-1797. [27] Li, S.; Zhan, L.; Liu, F.; Ren, J.; Shi, M.; Li, C.-Z.; Russell, T. P., Chen, H. An Unfused-Core-Based Nonfullerene Acceptor Enables High-Efficiency Organic Solar Cells with Excellent Morphological Stability at High Temperatures. *Adv. Mater.* **2018**,*30*, 1705208. [28] Huang, H.; Guo, Q.; Feng, S.; Zhang, C.; Bi, Z.; Xue, W.; Yang, J.; Song, J.; Li, C.; Xu, X.; Tang, Z.; Ma, W., Bo, Z. Noncovalently fused-ring electron acceptors with near-infrared absorption for high-performance organic solar cells. *Nat. Commun.* **2019**,*10*, 3038. [29] Liu, X.; Wei, Y.; Zhang, X.; Qin, L.; Wei, Z., Huang, H. An A-D-A'-D-A type unfused nonfullerene acceptor for organic solar cells with approaching 14% efficiency.

Sci. China Chem. **2021**,*64*, 228-231. [30] Zhang, X.; Qin, L.; Yu, J.; Li, Y.; Wei, Y.; Liu, X.; Lu, X.; Gao, F., Huang, H. High-Performance Noncovalently Fused-Ring Electron Acceptors for Organic Solar Cells Enabled by Noncovalent Intramolecular Interactions and End-Group Engineering. *Angew. Chem. Int. Ed.***2021**, *60*, 12475-12481. [31] Zhang, X.; Li, C.; Qin, L.; Chen, H.; Yu, J.; Wei, Y.; Liu, X.; Zhang, J.; Wei, Z.; Gao, F.; Peng, Q., Huang, H. Side-Chain Engineering for Enhancing the Molecular Rigidity and Photovoltaic Performance of Noncovalently Fused-Ring Electron Acceptors. *Angew. Chem. Int. Ed.* **2021**, *60*, 17720-17725. [32] Bai, Q.; Liang, Q.; Li, H.; Sun, H.; Guo, X., Niu, L. Recent progress in low-cost noncovalently fused-ring electron acceptors for organic solar cells. *Aggregate* **2022**, *3*, e281. [33] Gu, X.-B.; Gao, J.-H.; Han, Z.-Y.; Shi, Y.-H.; Wei, Y.-N.; Zhang, Y.-C.; Peng, Q.; Wei, Z.-X.; Zhang, X., Huang, H. A Simple Building Block with Noncovalently Conformational Locks towards Constructing Low-Cost and High-Performance Nonfused Ring Electron Acceptors. *Chin. J. Polym. Sci.* **2023**, *41*, 556-563. [34] Yu, Z.-P.; Liu, Z.-X.; Chen, F.-X.; Qin, R.; Lau, T.-K.; Yin, J.-L.; Kong, X.; Lu, X.; Shi, M.; Li, C.-Z., Chen, H. Simple non-fused electron acceptors for efficient and stable organic solar cells.*Nat. Commun.* **2019**, *10*, 2152. [35] Ma, L.; Zhang, S.; Zhu, J.; Wang, J.; Ren, J.; Zhang, J., Hou, J. Completely non-fused electron acceptor with 3D-interpenetrated crystalline structure enables efficient and stable organic solar cell.*Nat. Commun.* **2021**, *12*, 5093. [36] Wang, X.; Lu, H.; Liu, Y.; Zhang, A.; Yu, N.; Wang, H.; Li, S.; Zhou, Y.; Xu, X.; Tang, Z., Bo, Z. Simple Nonfused Ring Electron Acceptors with 3D Network Packing Structure Boosting the Efficiency of Organic Solar Cells to 15.44%. *Adv. Energy Mater.* **2021**,*11*, 2102591. [37] Huang, H.; Chen, Z.; Ortiz, R. P.; Newman, C.; Usta, H.; Lou, S.; Youn, J.; Noh, Y.-Y.; Baeg, K.-J.; Chen, L. X.; Facchetti, A., Marks, T. Combining Electron-Neutral Building Blocks with Intramolecular "Conformational Locks" Affords Stable, High-Mobility P- and N-Channel Polymer Semiconductors. *J. Am. Chem. Soc.* **2012**,*134*, 10966-10973. [38] Huang, H.; Yang, L.; Facchetti, A., Marks, T. J. Organic and Polymeric Semiconductors Enhanced by Noncovalent Conformational Locks.*Chem. Rev.* **2017**, *117*, 10291-10318. [39] Han, Z.; Li, C.; Gu, X.; Han, X.; Wang, S.; Wei, Y.; Gao, J.; Wei, Z.; Cai, Y.; Zhang, X., Huang, H. Combination of S***N and S***Cl Noncovalently Conformational Locks for Constructing High-Planarity and Low-Cost Nonfused-Ring Electron Acceptors+. *Chin. J. Chem.***2023**, *41*, 1797-1802. [40] Gu, X.; Wei, Y.; Liu, X.; Yu, N.; Li, L.; Han, Z.; Gao, J.; Li, C.; Wei, Z.; Tang, Z.; Zhang, X., Huang, H. Low-cost polymer acceptors with noncovalently fused-ring backbones for efficient all-polymer solar cells. *Sci. China Chem.* **2022**, *65*, 926-933. [41] Gu, X.; Wei, Y.; Yu, N.; Qiao, J.; Han, Z.; Lin, Q.; Han, X.; Gao, J.; Li, C.; Zhang, J.; Hao, X.; Wei, Z.; Tang, Z.; Cai, Y.; Zhang, X., Huang, H. High-Efficiency and Low-Energy-Loss Organic Solar Cells Enabled by Tuning Conformations of Dimeric Electron Acceptors. *CCS Chem.* **2023**, DOI: 10.31635/ccschem.31023.202202575. [42] Gu, X.; Wei, Y.; Lu, G.; Han, Z.; Zheng, D.; Lu, G.; Zhang, J.; Wei, Z.; Cai, Y.; Zhang, X., Huang, H. Insight into the efficiency-stability-cost balanced organic solar cell based on a polymerized nonfused-ring electron acceptor. *Aggregate***2023**, DOI: 10.1002/agt1002.1388. [43] Li, C.; Zhang, X.; Yu, N.; Gu, X.; Qin, L.; Wei, Y.; Liu, X.; Zhang, J.; Wei, Z.; Tang, Z.; Shi, Q., Huang, H. Simple Nonfused-Ring Electron Acceptors with Noncovalently Conformational Locks for Low-Cost and High-Performance Organic Solar Cells Enabled by End-Group Engineering. *Adv. Funct. Mater.* **2022**, *32*, 2108861.

Manuscript received: XXXX, 2023 Manuscript revised: XXXX, 2023 Manuscript accepted: XXXX, 2023 Accepted manuscr

Entry for the Table of Contents

Enhancing Photovoltaic Performance of Nonfused-Ring Electron Acceptors via Asymmetric End-group Eng

The asymmetric end-group engineering was employed to construct a new nonfused-ring electron acceptors (NFREAs), name